Vol. 04, Iss. 3 (2026) 364-377, DOI: 10.61552/JME.2026.03.006

JME

Journal of Materials and Engineering

www.jme.aspur.rs

Research article

Dimple Formation and Squeeze-Out of Resistive Powder in Hertzian Contacts

Marco Bruno[a,*], Luigi Portaluri[a], Michele Scaraggi[a,b,c,*]

[a]*Università del Salento, Department of Engineering for Innovation, Lecce, Italy,*
[b]*Istituto Italiano di Tecnologia, Center for Biomolecular Nanotechnologies, Arnesano, Italy,*
[c]*State Key Laboratory of Solid Lubrication, Lanzhou Institute of Chemical Physics, Chinese Academy of Sciences, Lanzhou, China.*

Keywords:

Dimple formation
Electrical contact resistance
Granular interlayer
Fe_3O_4 nanoparticles
Hertzian contact
Powder compaction
Contact area
Frustrated total internal reflection

* Corresponding author:

Marco Bruno
E-mail: marco.bruno@iit.it
Michele Scaraggi
Email: michele.scaraggi@unisalento.it

Received: 5 June 2026
Revised: 1 July 2026
Accepted: 14 August 2026

A B S T R A C T

Electrical contact resistance in powder-mediated interfaces is governed by the coupled evolution of roughness-induced contact area formation, particle rearrangement, compaction and current-path connectivity. This work investigates the normal indentation of a resistive Fe_3O_4 nanoparticle layer confined between a spherical steel indenter and a molybdenum-coated glass substrate. Contact resistance was measured under increasing normal force while the contact morphology was imaged from below using frustrated total internal reflection. The resistance decreased systematically with load, indicating progressive activation of conducting pathways through the granular interlayer. Optical images revealed an annular bright region surrounding a darker central zone, suggesting the formation of a dimple-like contact morphology. This observation is interpreted as the coexistence of a confined, solid-like granular core and an annular region that is rearranging during the indenter approach. A simplified contact-resistance model was introduced by combining Hertzian theory, multiscale rough contact mechanics and a first-order thickness contribution. The model captures the main resistance decrease for selected powder layers but cannot fully describe the strong sensitivity to layer thickness. The results suggest that dimple formation and contact-network evolution are key mechanisms in squeezed resistive powder contacts.

1. INTRODUCTION

Electrical contact resistance is a central problem in tribology, electrical connectors, powder metallurgy, batteries, sensors and electrochemical interfaces. When two nominally solid conductors are pressed together, the current does not pass uniformly through the contact area at the scale of observation. Instead, it is constricted through a population of small load-bearing regions, producing an additional resistance that depends on the local geometry and mechanics of the interface. The classical theory of electrical contacts was developed by Holm, who related contact resistance to the constriction of current through isolated contact spots [1]. Greenwood later extended this view to clusters of circular conducting spots and showed that the electrical resistance of a multi-contact interface cannot be obtained simply by adding independent single-spot resistances [2]. In parallel, Greenwood and Williamson introduced a statistical model for rough elastic contacts in which the real contact area emerges from the deformation of asperities with distributed heights [3], the so-called multi-asperity contact formalism. These works established the central idea that contact resistance is determined by the microscopic structure of the load-bearing interface, not solely by the nominal contact geometry.

More recent contact-resistance models have refined this view by linking electrical conductance to contact mechanics at multiple length scales. Barber developed bounds for the electrical resistance between elastic rough bodies and showed that conductance can be related to the mechanical compliance of the interface [4]. Persson subsequently discussed the relation between the classical Holm-type constriction picture and the stiffness-based formulation of electrical contact resistance [5]. These models are powerful for clean metallic or elastic rough contacts, but their direct application to powder-mediated contacts is not straightforward.

A compressed powder interlayer introduces additional mechanisms that are absent in classical rough contacts [6, 7]. The current may pass through particle-particle junctions, particle-electrode junctions, oxide or contamination layers, so that a disordered network of conducting and poorly conducting paths can be expected. The resistance of a powder compact is therefore affected by porosity, coordination number, packing heterogeneity, particle morphology, surface (e.g. contaminants) films and the history of compression [8, 7]. Compressed powders and granular conductors usually exhibit an increasing electrical conductivity with pressure, because compaction reduces porosity and increases the number and overall area of particle contacts [9, 10]. Network and percolation descriptions are therefore often more appropriate than a simple homogeneous-film resistivity model [11].

Granular materials are neither ordinary solids nor ordinary fluids. Depending on confinement, shear stress and packing state, a dense granular medium may remain jammed, flow plastically, or rearrange through localized shear. The dense-flow constitutive law proposed by Jop, Forterre and Pouliquen provided a continuum description in which granular flow is governed by a friction coefficient depending on the inertial number [12]. Moreover, pressure-dependent friction and solid-fluid transitions are typical features of granular media [11]. Metallic granular media can also show nonlinear, history-dependent and stress-dependent electrical transport because oxide films, microwelding, contact aging and network rearrangement affect the conducting paths [13, 14, 15]. In addition, depending on the indenter geometry, regions with different mechanical states can form within the contact region: A highly confined core may remain jammed, while surrounding regions may rearrange or flow depending on the local stress condition [12, 16, 17].

A related phenomenon is well known in squeezed lubricated contacts. In squeeze-film and elastohydrodynamic lubrication (EHL), the drainage of a viscous fluid trapped between approaching surfaces can generate a central dimple or squeeze-cave profile [18]. Such dimples have been observed and modelled in soft- [19] as well as hard-EHL contacts [20, 21]. Transient dimple evolution under combined entraining and squeeze-film motion has also been analyzed in elastohydrodynamic point contacts [22], while a broader overview of transient phenomena in elastohydrodynamic lubrication is provided in [23]. In these systems, dimple formation is usually associated with fluid pressurization, elastic deformation and delayed drainage from the contact centre. Similar dimple-like profiles have also been discussed in air cushioning during droplet impact and in soft lubrication problems, where a trapped fluid layer delays full contact [24]. However, these studies concern liquid or gas films, not dry granular layers. To the best of the authors' knowledge, dimple-like contact morphology in a squeezed powder interlayer has not been directly reported in the literature.

The present work investigates the dimple formation in the squeeze-out of powder compressed in between elastic Hertzian contacts, using Fe_3O_4 nanoparticle layers confined between a steel spherical indenter and a molybdenum-coated glass substrate. The goal is not to characterize a specific functional oxide, but to study how a resistive granular interlayer modifies the contact interface morphology and electrical resistance under normal loading, and to report the first observation, to the best of the authors' knowledge, of dimple formation in the squeeze-out of granular material. A frustrated total internal reflection configuration is used to image the apparent contact from below, whereas the electrical resistance is measured between the indenter and a conductive substrate.

The experiments reveal a systematic decrease in resistance with normal load and the occurrence of an annular optical feature interpreted as a dimple-like interface morphology. A reduced resistance model is then introduced by combining Hertzian apparent contact growth, pressure-dependent activation of conducting microcontacts and a simplified thickness-dependent contribution.

This framework provides a first phenomenological link between granular contact morphology and force-dependent electrical resistance in squeezed granular layers, which is critical in the design of electrochemical interfaces such as batteries and fuel cells. Moreover, the study highlights the limitations of treating the powder as either a homogeneous conducting film or a classical rough metallic contact, suggesting that novel modelling strategies are needed to capture the complexities occurring in the contact mechanics of granular material.

2. MATERIALS AND METHODS

2.1 Materials and substrate preparation

Iron(II,III) oxide nanopowder (Fe_3O_4, Sigma-Aldrich product 637106, nominal particle size 50-100 nm) was used as the conductive granular interlayer. Glass slides were coated with molybdenum by sputtering to obtain a conductive bottom electrode. Molybdenum was selected because sputtered Mo films can provide low-resistance conductive coatings on glass with good mechanical robustness.

Before sputtering, glass slides were rinsed with acetone and isopropanol and dried with nitrogen. Molybdenum was deposited in argon at $5 \cdot 10^{-3}$ mbar, 200 W sputtering power, room temperature, and 30 min deposition time. The nominal film thickness was 260 nm. No post-treatment was applied.

2.2 Powder deposition

Fe_3O_4 powder was dispersed in deionized water at 10 mg/mL and sonicated for 5 min before deposition. Before each deposition step, the vial was gently agitated to reduce sedimentation effects. A 20 μL droplet was deposited on the Mo-coated glass substrate and dried on a hot plate at 100 °C under magnetic stirring to reduce large cluster formation. Three powder-coated regions, denoted V1, V2 and V3, were prepared and tested. The deposited powder regions and their corresponding profilometry maps are shown in Fig. 1.

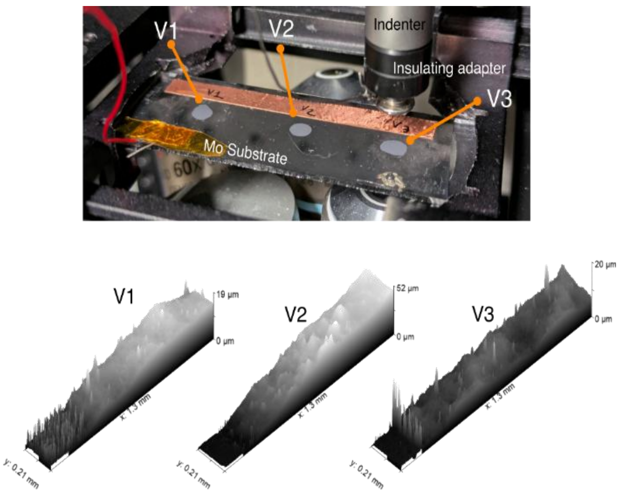

Fig. 1. Powder deposition (top) and layer morphology (bottom). Top: photograph of the Mo-coated glass substrate after Fe_3O_4 deposition, showing the three tested powder regions V1, V2 and V3 and the electrically insulated spherical indenter. Bottom: optical profilometry maps of the deposited powder regions, showing the nonuniform thickness and surface morphology of the granular interlayers.

The representative thickness and RMS areal roughness of each powder layer were extracted from the profilometry maps using a $100 \times 200\,\mu m^2$ rectangular mask. The mask was positioned near the edge of the profilometry scan, sufficiently far from the layer edges to avoid the boundary variations. The representative thickness was calculated as the arithmetic mean of all height points within the mask, whereas the RMS areal roughness, S_q, was calculated from the height fluctuations in the same region. The resulting values were $t = 12.98\,\mu m$ and $S_q = 1.58\,\mu m$ for V1, $t = 44.95\,\mu m$ and $S_q = 5.90\,\mu m$ for V2, and $t = 7.33\,\mu m$ and $S_q = 1.20\,\mu m$ for V3.

2.3 Mechanical loading and electrical measurement

The experimental platform combined a motorized indentation head, a force sensor, laser displacement sensors, an electrical measurement circuit and an inverted microscope. The integrated experimental configuration is shown in Fig. 2. Steel spherical indenters were mounted using an electrically-insulating adapter so that the indenter could act as the top electrode. The contact-resistance measurements reported here were performed using a 2 mm diameter steel sphere.

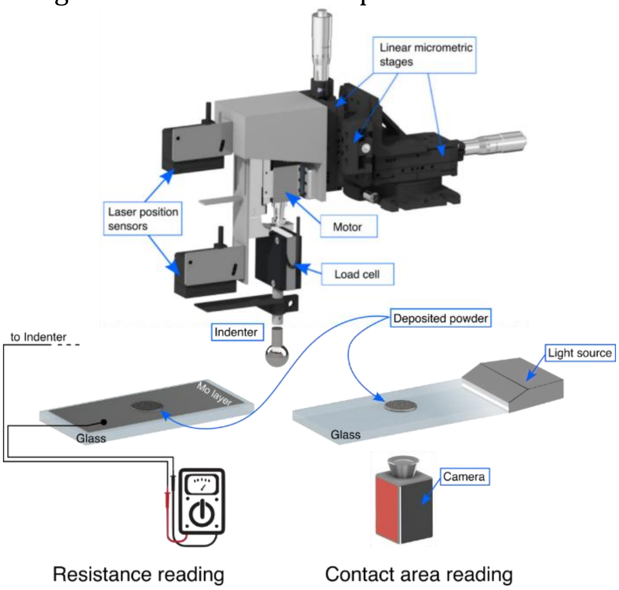

Fig. 2. Schematic of the experimental setup for the contact-resistance measurement and optical contact imaging. A spherical steel indenter is mounted on an electrically-insulated loading head and pressed against a Fe_3O_4 powder layer deposited on a molybdenum-coated glass substrate. The indenter and the Mo coating act as the top and bottom electrodes, respectively, while the contact region is imaged from below using frustrated total internal reflection.

Additional optical contact-area observations were acquired using 2, 4 and 5.5 mm diameter spheres to compare the apparent contact morphology with the Hertzian size estimate. Normal loading was imposed stepwise using a custom LabVIEW control software. The normal-force sequence used for the resistance measurements was 0.12, 0.25, 0.50 and 1.00 N. One loading sequence was performed for each powder region. At each force level, resistance acquisition began immediately upon reaching the prescribed force level and continued throughout the subsequent force-hold interval. The recorded interval was not fixed because the time required to stabilize the reading varied with powder layer thickness and force level. The mean resistance and temporal standard deviation were calculated from the individual source-meter updates recorded during each interval. The numbers of readings were, respectively, 84, 92, 121 and 105 for V1; 78, 76, 69 and 83 for V2; and 165, 578, 452 and 648 for V3. At each step, the force was held while the electrical resistance or optical contact image was acquired. The resistance and optical acquisitions of the contact were acquired in separate but identical loading sequences. Resistance was measured between the steel indenter and the molybdenum-coated glass substrate using a Keithley 2400 Source-meter in a two-wire configuration.

Measurements were performed at 10 V, and the resistance was extracted from the current-voltage response after signal stabilization. The parasitic resistance measured by direct contact between the indenter and the Mo-coated glass was approximately 100 Ω near the tested regions, much lower than the powder-mediated contact resistance, indicating that a two-wire configuration introduced negligible differences in the overall resistance readings.

2.4 Optical contact imaging

The apparent contact region was imaged using a frustrated total internal reflection configuration. Light was coupled into the glass slide from the side. When powder grains or the indenter approached the glass surface within the evanescent-field range, total internal reflection was locally frustrated, and the emitted light was collected by the microscope objective. In rough elastic contacts, brighter regions correspond to higher pressure regions, because of a smaller locally-averaged gap between the glass and the contacting object. In powder-mediated contacts, this argument is no longer valid due to the fluid-like behaviour of the powder medium. The interpretation is therefore more qualitative: Brighter regions can only be interpreted as lower-gap regions, not necessarily at high pressure. Indeed, one can expect that, near the Hertzian contact radius, the lower contact pressure allows the granular material to get more compacted (thus with a reduced locally-averaged separation near the evanescent-field range) and squeeze out much like a fluid in a hEHL normal contact. The images were therefore used to identify apparent contact growth and powder redistribution, rather than to directly extract a pressure map.

3. EXPERIMENTAL RESULTS

3.1 Contact morphology

Optical acquisitions of powder-mediated contacts revealed an unconventional tribological behaviour. At increasing loads, an annular bright region appeared around a central contact zone. This evolution is shown in Fig. 3, where the powder-mediated contacts are compared with the Hertzian contact estimate (the same predicted contact radii are reported quantitatively in Table 1) and with a reference contact without powder. Because the FTIR intensity was not calibrated against local separation, it is not possible to measure quantities such as the local gap and the actual contact radius. The Hertzian radius is therefore reported as a quantitative reference, while the evolution of the experimental annular morphology can be interpreted only qualitatively.

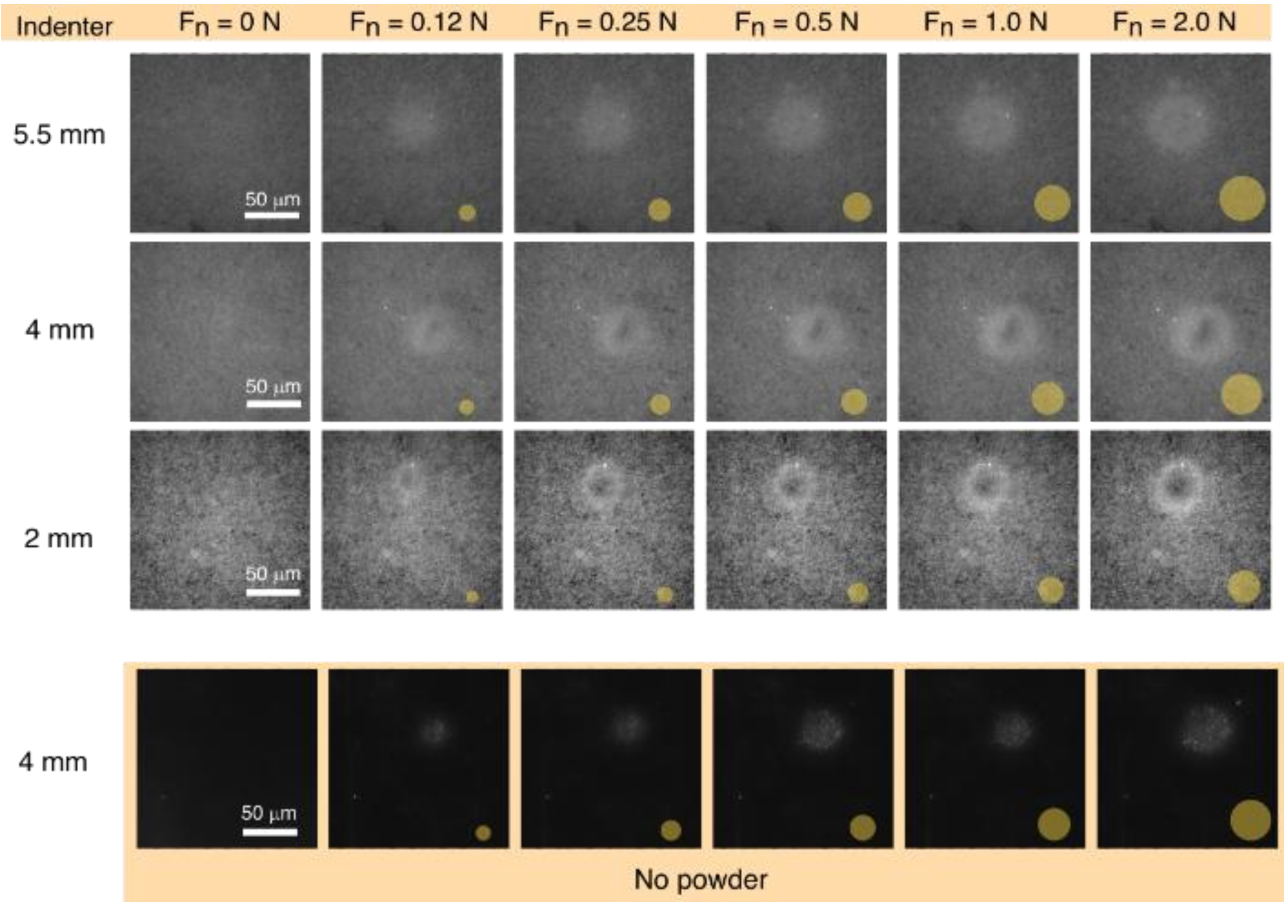

Fig. 3. Optical contact images acquired under increasing normal force. Frustrated total internal reflection images are shown for powder-mediated contacts (top three rows) and for a reference contact without powder (bottom row). The yellow disks indicate the Hertzian contact size estimated from the applied load, indenter geometry and material properties. In the powder-mediated contacts, the optical signal develops an annular bright region, indicating a nonuniform powder rearrangement at the contact interface.

Table 1. Theoretical Hertzian contact radius for the three steel sphere diameters at increasing normal force. Values are reported in μm.

Force (N)	D=2 mm	D=4mm	D=5.5 mm
0.12	24	30	33
0.25	30	38	43
0.50	38	48	54
1.00	48	61	68
2.00	61	77	85

A direct interpretation is that the granular layer experiences different confinement states within the apparent contact. The central region is subjected to a more hydrostatic stress state, which clamps the particles (due to inter-particle friction) and limits lateral rearrangement. Near the contact edge, shear and reduced confinement facilitate grain redistribution, producing a plastic-like annular zone with increased granular compaction. The increased compaction is equivalent to lowering the locally-averaged contact gap at the interface with the glass slide, thus increasing light frustration. The proposed interpretation of this morphology is summarized schematically in Fig. 4.

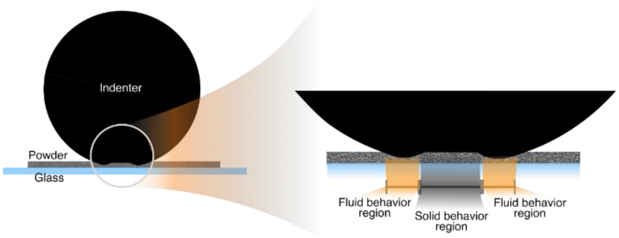

Fig. 4. Proposed dimple-like morphology formation in a squeezed granular interlayer. The central region of the powder layer is confined under relatively high pressure and behaves as a jammed, solid-like zone. The outer annular region is less hydrostatically constrained and can rearrange and locally flow, producing the bright annular feature observed in the optical contact images due to the smaller locally averaged separation within the evanescent-field range.

This observation is consistent with a dimple-like contact morphology typically occurring in the squeeze-out EHL, where a central oil dimple is formed (e.g. because of piezoviscosity in the case of hEHL) with gap thickness higher than the gap close to the Hertzian contact radius. Therefore, these results show that a powder layer behaves as a deformable third body whose local effective viscosity shows a piezoviscous-like behaviour, driven by the internal particle-particle friction and driving its compaction morphology.

3.2 Electrical resistance vs squeeze force

All powder regions showed a monotonic decrease in resistance with increasing normal force, indicating progressive activation of conducting pathways. The response, however, depended strongly on the deposited region. V1 and V3 showed comparable load-dependent trends, whereas V2 (thicker deposited layer) exhibited much higher resistance over the same force range. The force-resistance curves are reported in Fig. 5 together with the model comparison discussed below. Given that V2 is also the thickest powder region, this result indicates that nominal thickness affects resistance not only through a simple longer conduction path, but also through changes in packing, connectivity and compaction state. The resistance values used for model comparison were extracted from the tests shown in Fig. 5, the average (standard deviation) values are summarized in Table 2.

Table 2. Resistance values averaged over the acquisition interval immediately following attainment of each target force. Values (standard deviation) are reported in kΩ.

Force (N)	V1	V2	V3
0.12	30.43 (0.37)	648.79 (7.04)	8.90 (0.31)
0.25	13.68 (0.11)	218.70 (1.99)	5.11 (0.29)
0.50	6.03 (0.05)	101.12 (0.52)	3.47 (0.03)
1.00	2.64 (0.01)	36.91 (0.17)	1.35 (0.03)

4. CONTACT-RESISTANCE MODEL

The contact-resistance measurements are interpreted using a simplified contact model. In classic particle-resolved electro-mechanical models, the powder layer is represented as a discrete contact network in which electrical transfer occurs through particle-particle and particle-wall junctions.

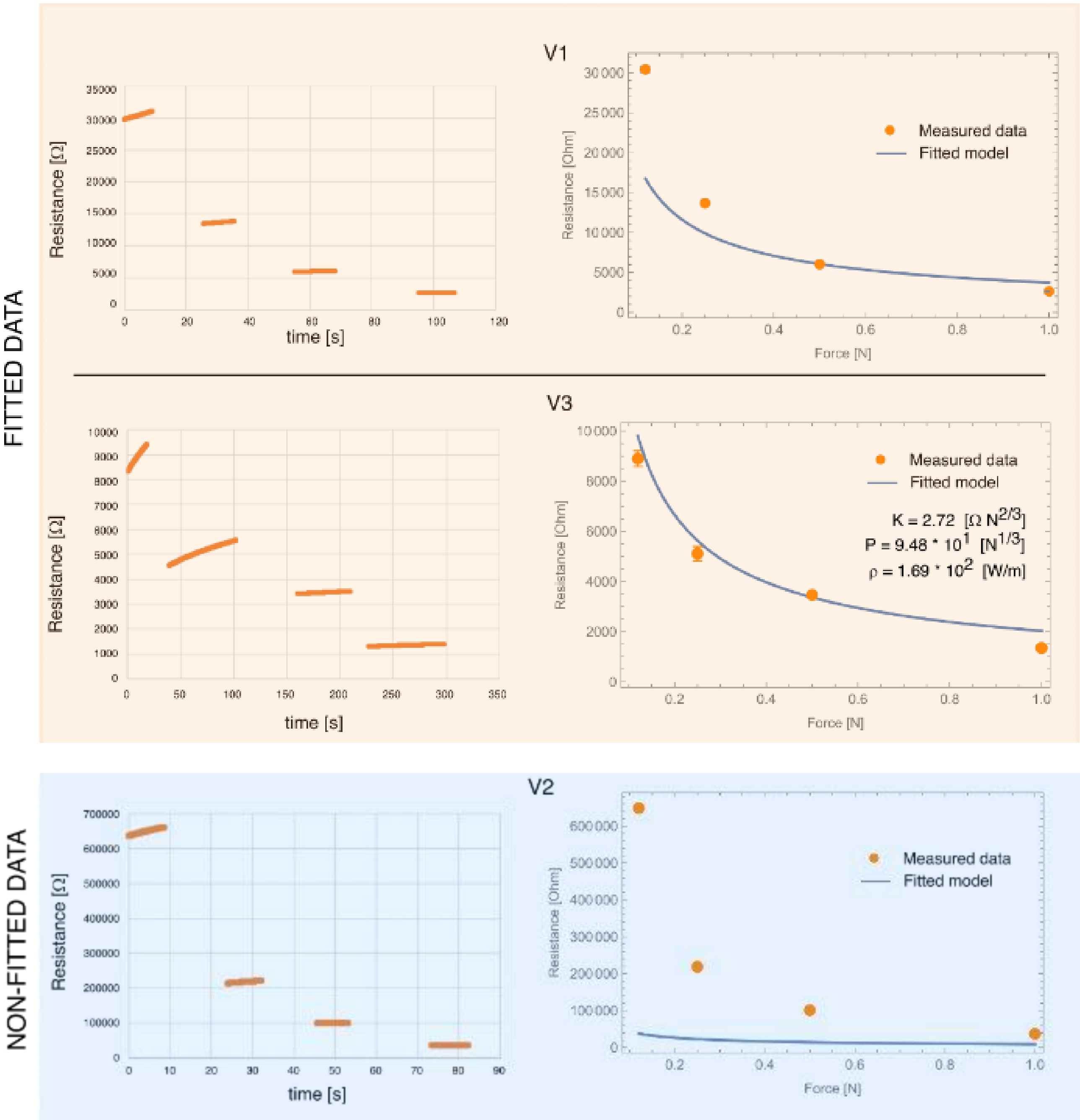

Fig. 5. Contact-resistance measurements and model comparison. Left panels: resistance measured during stepwise loading of the V1, V2 and V3 powder regions. Right panels: comparison between experimental resistance values and the reduced contact-resistance model. The fitting was performed using V1 and V3, while V2 was excluded because its much higher resistance suggests additional thickness, packing or connectivity effects not captured by the first-order model.

Depending on the formulation, the local conductance can be related to normal contact force, Hertzian contact radius, constriction resistance, or prescribed junction laws, while the global resistance is obtained by solving the resulting resistor network. These methods are well-suited to study the role of packing geometry, contact connectivity, and particle rearrangement, but they require assumptions on particle shape, size distribution, contact mechanics, and junction resistance [25, 26, 27, 28]. The present work, therefore, uses a reduced active-area multiscale model calibrated from force-resistance data, while treating unresolved granular-network effects through effective parameters. The objective is to relate the measured resistance to the load-dependent electrically active area formed inside the apparent Hertzian contact. The model is not intended to extract an intrinsic resistivity of the powder. Instead, it provides a mechanically constrained phenomenological description of a granular interlayer whose conducting network evolves under compression. The modelling chain is:

$$F \rightarrow A_{\text{app}}(F) \rightarrow A_{\text{real}}(F) \rightarrow R(F,t) \quad (1)$$

where F is the applied normal force, A_{app} is the apparent contact area, A_{real} is the electrically active real contact area, R is the measured resistance, and t is the nominal powder-layer thickness. The formulation is based on four assumptions. First, the outer contact radius is approximated by Hertz theory. Second, only a pressure-dependent fraction of the apparent contact conducts current. Third, the granular layer contributes with a finite thickness-dependent resistance. Fourth, particle-scale processes such as packing, agglomeration, local rearrangement and particle junction activation are absorbed into effective parameters.

4.1 Hertzian apparent contact

The apparent contact is estimated from Hertz theory [29, 30] for a spherical indenter pressed against an elastic half-space. This approximation is used only to describe the outer scale of the contact. The powder layer can rearrange locally, but the spherical geometry still provides a useful estimate of the load-dependent apparent contact size. The apparent contact radius is

$$a(F) = \left(\frac{3FR}{4E_{\text{eff}}}\right)^{1/3} \quad (2)$$

where R is the radius of the spherical indenter and E_{eff} is the effective elastic modulus of the contacting system. The corresponding apparent contact area is

$$A_{\text{app}}(F) = \pi a^2(F) \quad (3)$$

and therefore, as well known,

$$A_{\text{app}}(F) \propto F^{2/3}. \quad (4)$$

The Hertz pressure is not uniform inside the apparent contact. It varies radially as

$$p_{\text{H}}(r,F) = p_{\max}(F)\sqrt{1-\frac{r^2}{a^2(F)}} \quad (5)$$

where

$$p_{\max}(F) = \frac{3F}{2\pi a^2(F)}. \quad (6)$$

Since $a(F) \propto F^{1/3}$, the maximum Hertz pressure scales as

$$p_{\max}(F) \propto F^{1/3}. \quad (7)$$

This pressure scaling is used below to describe the load-dependent activation of conducting pathways in the powder-mediated interface.

4.2 Pressure-activated real conducting area

The electrical current is assumed not to cross the entire apparent contact area.

In a powder-mediated interface, only part of the apparent Hertzian region contains load-bearing and electrically active particle-particle, particle-indenter and particle-substrate junctions. This active fraction is described using Persson's multiscale rough contact mechanics [31] .

In this formulation, increasing the magnification ζ progressively resolves finer roughness wavelengths. Each newly resolved roughness band introduces additional local pressure fluctuations, so the probability density $\mathcal{P}(p,\zeta)$ of local pressures broadens in pressure space according to

$$\frac{\partial \mathcal{P}}{\partial \zeta} = \frac{1}{2}\frac{dG(\zeta)}{d\zeta}\frac{\partial^2 \mathcal{P}}{\partial p^2}. \quad (8)$$

Here p is the local pressure and $G(\zeta)$ is the accumulated variance of the pressure fluctuations generated by the resolved roughness. Since G has units of pressure squared, it is convenient to define an effective activation pressure scale

$$p_{\text{c}} = \sqrt{2G(\zeta_1)} \quad (9)$$

where ζ_1 is the largest resolved magnification, treated here as an effective upper roughness frequency cutoff. For a non-adhesive interface, regions whose local pressure reaches zero are considered out of contact. This leads to the local active-area fraction

$$\eta(p) = \text{erf}\left(\frac{p}{p_{\text{c}}}\right). \quad (10)$$

For the present powder-mediated interface, p_c is not calculated directly from a measured surface power spectrum. Instead, it is treated as an effective pressure scale that includes powder roughness, packing density, agglomeration, local compliance, particle rearrangement and particle-level contact activation.

For a Hertzian contact, the local mean pressure is not constant. The active fraction must therefore be integrated over the apparent contact disk:

$$A_{\mathrm{real}}(F) \approx \int_0^{a(F)} 2\pi r \,\mathrm{erf}\left[\frac{p_{\mathrm{H}}(r,F)}{p_{\mathrm{c}}}\right] dr. \quad (11)$$

Substitution of Eq. (5) into Eq. (11) gives

$$A_{\mathrm{real}}(F) = A_{\mathrm{app}}(F)\,\Phi[\alpha(F)] \quad (12)$$

where

$$\alpha(F) = \frac{p_{\max}(F)}{p_{\mathrm{c}}} \quad (13)$$

and the Hertz-local correction factor can be written as

$$\Phi(\alpha) = 2\int_0^1 u\ \mathrm{erf}\big(\alpha\sqrt{1-u^2}\big)du. \quad (14)$$

Evaluation of the integral gives

$$\Phi(\alpha) = \left(1 - \frac{1}{2\alpha^2}\right)\mathrm{erf}(\alpha) + \frac{\exp(-\alpha^2)}{\sqrt{\pi}\,\alpha}. \quad (15)$$

The function $\Phi(\alpha)$ is the average active fraction over the Hertzian disk. It differs from a simpler mean-pressure expression because the Hertz contact contains a high-pressure centre and a low-pressure edge.

4.3 Resistance model

The measured resistance is assumed to arise from two load-dependent contributions. The first contribution is associated with the formation of electrically active microcontacts inside the apparent Hertzian contact region. The second contribution accounts, in a first-order way, for the finite resistance of the powder interlayer through its thickness. The total resistance is therefore written as

$$R(F,t) = \frac{\rho_{\mathrm{c}}}{A_{\mathrm{real}}(F)} + \frac{\rho_{\mathrm{b}}\,t}{A_{\mathrm{app}}(F)} \quad (16)$$

where ρ_c is an effective contact-resistance coefficient and ρ_b is an effective thickness-resistance coefficient. The first term includes particle-particle, particle-indenter and particle-substrate junctions, together with constriction effects inside the activated contact network. The second term represents a simplified bulk-like contribution of the powder layer. It should not be interpreted as proof that the powder behaves as a homogeneous film; rather, it accounts for the fact that thicker deposits can introduce longer, more tortuous and less compacted current paths.

Using the Hertz-local real-area correction of Eq. (12), Eq. (16) becomes

$$R(F,t) = \frac{\rho_{\mathrm{c}}}{A_{\mathrm{app}}(F)\,\Phi[\alpha(F)]} + \frac{\rho_{\mathrm{b}}\,t}{A_{\mathrm{app}}(F)} \quad (17)$$

Equation (17) separates two contact effects. The apparent Hertzian area increases with force, while the pressure-dependent activation factor increases the electrically active fraction of that area. The thickness term retains the same inverse-area scaling but does not contain Φ, because it is treated as a first-order contribution through the already confined granular layer.

This formulation assumes that the electrically active fraction increases monotonically with local pressure, following a solid-like rough-contact description. It does not account for a spatial transition from a jammed central region to a rearranging granular peripheral region, in which the number of conducting paths may evolve independently of the instantaneous pressure. In the high-pressure central region, the existing junctions may become more conductive as pressure increases, but the strongly confined, jammed state limits particle rearrangement and the formation of new contact spots. Near the contact boundary, the lower confinement allows plastic-like granular rearrangement, which may increase the number of particle-particle and particle-electrode contacts despite the lower local pressure. The model should therefore be regarded as a first-order approximation of the overall resistance response rather than as a local map of electrical conductance.

4.4 Reduced fitting form

For the fitting implementation, the Hertz scaling of the apparent contact area is retained while the unknown proportionality constants are absorbed into empirical parameters. Since

$$A_{\mathrm{app}}(F) \propto F^{2/3}, \qquad \alpha(F) \propto F^{1/3} \tag{18}$$

the model can be expressed in reduced form as

$$R(F,t) = \frac{K}{F^{2/3}\,\Phi\left(F^{1/3}/P\right)} + \frac{\rho\, t}{F^{2/3}}. \tag{19}$$

Equivalently, defining the reduced Hertz-local activation factor as

$$\Phi_R(F;P) = \left(1 - \frac{P^2}{2F^{2/3}}\right)\mathrm{erf}\left(\frac{F^{1/3}}{P}\right) + \frac{P\exp\left(-F^{2/3}/P^2\right)}{\sqrt{\pi}\,F^{1/3}} \tag{20}$$

the fitted resistance law is

$$R(F,t) = \frac{K}{F^{2/3}\Phi_R(F;P)} + \frac{\rho\, t}{F^{2/3}}. \tag{21}$$

Here K is an effective contact-resistance scale, P is an effective activation parameter related to the pressure scale required to activate conducting powder contacts, and ρ is an effective coefficient associated with the thickness-dependent contribution. If F is expressed in N, then P has the dimensions of $F^{1/3}$ in the reduced fitting representation. The parameters K and ρ also carry empirical units set by the force and thickness units used in the fit. They absorb the Hertz prefactors, the effective modulus, the sphere radius, and sample-specific powder properties. Therefore, they should not be interpreted as intrinsic material properties unless the true current path, true contact area and powder packing state are independently known.

4.5 Fitting and prediction protocol

The model was fitted using the powder regions that showed comparable behavior and reliable resistance-force trends. In the present analysis, the V1 and V3 datasets were used for calibration because their thinner powder layers are more strongly confined between the opposing solid surfaces. This confinement limits internal particle rearrangement, making their response closer to that of a constrained granular solid. V2 was not treated as a statistical outlier; instead, it was retained as an out-of-calibration comparison representing a thicker and more rearrangement-prone granular layer. The same fitted parameters were therefore applied to V2 to assess the ability of the model to describe this different regime. Its deviation from the fitted response suggests that, as the layer thickness increases, network reorganization and the creation of additional conducting paths become increasingly important. Since these mechanisms are not explicitly represented by the present formulation, the model should be regarded as a first-order approximation applicable primarily to strongly confined powder layers. The nominal powder thicknesses used in the model were $t = 12.98\,\mu$m for V1, $t = 44.95\,\mu$m for V2 and $t = 7.33\,\mu$m for V3.

The parameters (K, P, ρ) were obtained by minimizing the squared error in logarithmic resistance over the V1 and V3 datasets:

$$\mathcal{L}(K,P,\rho) = \sum_{i\in\{V1,V3\}} \sum_{j=1}^{4}\left[\log R_{\mathrm{model}}\left(F_j, t_i; K, P, \rho\right) - \log R_{\mathrm{meas}}\left(F_j, t_i\right)\right]^2. \tag{22}$$

The logarithmic error was used because the resistance changes over a wide numerical range. This criterion is closer to minimizing relative error than absolute error and prevents the highest-resistance points from dominating the fit. After fitting, the same parameters were used to compare the model prediction with all available datasets.

This procedure tests whether the decrease in resistance with increasing normal force can be described by the combined effect of Hertzian growth of the apparent contact area, pressure-dependent activation of conducting microcontacts and a first-order thickness-dependent powder contribution. The comparison between fitted curves and experimental data is reported in Fig. 5.

The model captures the main resistance decrease for V1 and V3, but it does not fully describe the much larger resistance measured for V2. This indicates that the thickness dependence cannot be represented completely by a simple term proportional to t/A_{app}. The high resistance of the thicker powder region may involve additional effects, such as nonuniform powder coverage, incomplete compaction, agglomeration, poor particle-particle connectivity, lateral current spreading, or changes in the effective conduction path through the granular layer. Therefore, the present model should be considered a first-order phenomenological description. A more advanced model will be required to capture the strong resistance increase associated with powder thickness and to distinguish true bulk conduction from contact-network limitations.

4.6 Relation to contact-stiffness-based resistance models

In the classical constriction-resistance picture, the electrical response of a rough metallic contact is not governed only by the scalar real contact area. Persson, following Barber's argument, relates the interfacial electrical conductance to the normal contact stiffness through [4, 5]:

$$\alpha_{\mathrm{el}} = 2\sigma_{\mathrm{el,eff}} \frac{K_{\mathrm{N}}}{E_{\mathrm{eff}}} \tag{23}$$

where α_{el} is the electrical contact conductance per nominal area, $\sigma_{\mathrm{el,eff}}$ is the effective electrical conductivity, K_{N} is the normal interfacial contact stiffness and E_{eff} is the effective elastic modulus. This relation shifts the focus from the detailed population of microscopic contact spots to the mechanical compliance of the interface. In this framework, the constriction resistance is mainly controlled by the length scales that determine contact stiffness, often the long-wavelength roughness, rather than by the finest-scale real contact area alone.

The present powder-mediated contact does not satisfy the assumptions of a clean metallic constriction problem. The current path can be limited by particle-particle junctions, particle-electrode contacts, powder compaction, agglomeration and the finite resistance of the powder thickness. For this reason, the model used here does not attempt to infer the electrical resistance from contact stiffness. Instead, it writes the resistance as the sum of an active-area contribution and a thickness-dependent contribution, see (17). The first term represents the activation of conducting microcontacts inside the Hertzian apparent contact, while the second term introduces a first-order correction for the finite resistance of the granular layer. The advantage of this formulation is that it can be calibrated directly from the available force-resistance data and can include differences in nominal powder thickness. Its limitation is that the fitted parameters are effective quantities: They absorb contact activation, local packing, rearrangement, agglomerate fracture and current-path connectivity. Therefore, the model should be read as a compact phenomenological description of a granular interlayer, rather than as an alternative to the implementation of the contact-stiffness theory for clean rough metallic contacts, the latter inapplicable here.

5. DISCUSSION

A resistive powder interlayer develops a strongly load-dependent electrical response when confined between a spherical indenter and a conductive substrate. In all measured regions, the resistance decreased with increasing normal force, indicating the progressive activation of conducting pathways through the granular layer. Increasing load reduces void space, improves particle-particle and particle-electrode contacts, and creates additional parallel current paths. However, the resistance cannot be interpreted as the through-thickness resistance of a homogeneous film, because the current path is controlled by a disordered granular network made of constricted particle junctions, local packing variations, and evolving contact connectivity.

The optical observations show that the powder layer also undergoes a non-uniform mechanical rearrangement during indentation. The annular bright region observed in the contact images suggests a dimple-like morphology, with a confined central zone surrounded by a more mobile annular region. In classical FTIR contact imaging, higher brightness is often associated with smaller local gap or higher contact pressure. In the present case, the interpretation must be more cautious because the interlayer is granular and can scatter, compact, and rearrange under load. A plausible interpretation is that the central region becomes highly confined and solid-like, while the outer annular region is less hydrostatically constrained and can flow or plastically rearrange more easily. This interpretation is consistent with the coexistence of jammed and mobile regions in dense granular media.

This morphology is conceptually related to dimple formation in squeezed liquid and elastohydrodynamic contacts, where trapped fluid and delayed drainage produce a central dimple during compression. The present system differs because the interlayer is a dry granular powder rather than a viscous liquid film. The observation therefore suggests, for the first time to the best of the authors' knowledge, that dimple-like contact morphologies may also arise in squeezed granular interlayers when confinement, compaction, and shear-driven rearrangement coexist. In this sense, the dimple is not only a geometrical feature, but also a signature of the evolving mechanical state of the powder contact.

The resistance model provides a first-order interpretation of these coupled effects. The Hertzian apparent contact area describes the growth of the nominal contact region with load, while the pressure-activated area correction accounts for the fact that only part of this apparent contact is electrically active. This correction is important because the centre of a Hertzian contact reaches higher pressure than the edge and is therefore more likely to contain conducting microcontacts. The additional thickness-dependent term accounts for the finite resistance of the powder layer, but it should not be interpreted as a direct measurement of bulk resistivity. Its fitted value includes nonuniform coverage, tortuous current paths, particle junctions, local compaction, and geometrical prefactors.

The deviation of V2 is most plausibly related to powder rearrangement near the contact boundary. In this region, the lower confinement and the larger relative shear contribution allow the particles to slip and move outwards. As suggested by the annular morphology in Fig. 4, this redistribution allows the sphere to approach the substrate more closely near the contact edge, locally reducing the effective powder-layer thickness. The shorter conduction path, together with the formation of additional particle–particle and particle–electrode contacts, can reduce the resistance more strongly than predicted by a model based on a fixed representative thickness. This effect is restricted in thinner, strongly confined layers, whereas the greater thickness of V2 provides more freedom for particle slip and internal reconfiguration. The model captures the main resistance decrease for the V1 and V3 regions, which showed comparable force-resistance trends. However, it does not reproduce the much larger resistance measured in V2. This indicates that powder thickness does not act only as a simple conduction length proportional to the nominal layer thickness. A thicker layer can also modify packing density, compaction, agglomeration, lateral current spreading, and the connectivity of the conducting network. These effects are not included in the reduced model and probably explain the anomalous behaviour of V2.

The relation with contact-stiffness-based electrical resistance models is therefore indirect. In clean, rough metallic contacts, electrical conductance can be linked to the normal contact stiffness of the interface. In the present powder-mediated contact, mechanical compliance remains important, but the electrical response is also governed by particle rearrangement and network connectivity. For this reason, the active-area model should be read as a compact phenomenological description rather than as a direct implementation of classical metallic contact-resistance theory. A more predictive description would require a coupled granular-electrical model that determines the actual local pressure and powder-layer separation while accounting for particle slip, squeeze-out and the resulting evolution of conducting paths.

Overall, the results show that contact resistance in squeezed powder interlayers is controlled by the coupled evolution of contact morphology and electrical connectivity. The dimple-like annular structure indicates that granular flow and compaction are not secondary experimental artefacts, but central mechanisms governing the measured resistance.

6. CONCLUSION

This work investigated the contact morphology and electrical resistance of a squeezed resistive powder interlayer. Fe_3O_4 nanoparticles were deposited on molybdenum-coated glass and compressed with a spherical steel indenter under controlled normal loading. The setup combined force control, electrical resistance measurement and FTIR-based optical contact imaging, allowing the evolution of the granular contact to be followed during indentation.

The measured resistance decreased systematically with increasing normal force, confirming that compression activates additional conducting pathways through the powder layer. This response is attributed to the combined effects of apparent contact-area growth, particle rearrangement, powder compaction and improved particle-particle and particle-electrode connectivity. The optical images revealed an annular bright region around a less mobile central zone, interpreted as a dimple-like morphology in the squeezed granular layer. This suggests that the powder contact contains a highly confined, solid-like core surrounded by a more mobile annular region able to rearrange under load.

A reduced contact-resistance model was developed to interpret the force-resistance response. The model combines Hertzian apparent contact growth, a pressure-activated electrically active area and a first-order thickness-dependent resistance contribution. The Hertz-local correction accounts for the nonuniform pressure distribution inside the apparent contact and avoids treating the whole Hertzian area as uniformly conducting. The model captures the main resistance decrease for selected powder regions, but it does not reproduce the much higher resistance of the thickest region. This shows that powder thickness affects not only the geometric conduction length, but also packing, compaction, agglomeration and current-network connectivity.

The main contribution of this work is the identification of dimple-like morphology as a relevant feature of squeezed resistive powder contacts and its connection with force-dependent electrical resistance. The results support the view that powder-mediated contact resistance should be interpreted as a coupled tribological, granular and electrical-network problem. Future work should quantify the dimple geometry, extract active contact areas from optical images, perform controlled-thickness experiments, and develop coupled models able to describe granular compaction, rearrangement and electrical connectivity under load.

Acknowledgement

This work was supported by the project "BacForH2 – Celle a combustibile reversibili ad ossidi di elevata entropia per sistemi Power to Hydrogen", funded under the Italian PNRR – Missione 2, Componente 2, Investimento 3.5: Ricerca e sviluppo sull'idrogeno, within the NextGenerationEU programme, CUP F57G25000330006.

REFERENCES

[1] R. Holm, *Electric Contacts: Theory and Application*. Berlin, Heidelberg: Springer Berlin Heidelberg, 1967. doi: 10.1007/978-3-662-06688-1.

[2] J. A. Greenwood, "Constriction resistance and the real area of contact," *British Journal of Applied Physics*, vol. 17, no. 12, pp. 1621–1632, Dec. 1966, doi: 10.1088/0508-3443/17/12/310.

[3] J. A. Greenwood and J. B. P. Williamson, "Contact of nominally flat surfaces," *Proceedings of the Royal Society of London a Mathematical and Physical Sciences*, vol. 295, no. 1442, pp. 300–319, Dec. 1966, doi: 10.1098/rspa.1966.0242.

[4] J. R. Barber, "Bounds on the electrical resistance between contacting elastic rough bodies," *Proceedings of the Royal Society a Mathematical Physical and Engineering Sciences*, vol. 459, no. 2029, pp. 53–66, Jan. 2003, doi: 10.1098/rspa.2002.1038.

[5] B. N. J. Persson, "On the Electric Contact Resistance," *Tribology Letters*, vol. 70, no. 3, Jul. 2022, doi: 10.1007/s11249-022-01630-2.

[6] J. M. Montes, F. G. Cuevas, J. Cintas, and P. Urban, "Electrical conductivity of metal powders under pressure," *Applied Physics A*, vol. 105, no. 4, pp. 935–947, Jul. 2011, doi: 10.1007/s00339-011-6515-9.

[7] J. M. Montes, F. G. Cuevas, J. Cintas, and J. M. Gallardo, "Electrical conductivity of metal powder aggregates and sintered compacts," *Journal of Materials Science*, vol. 51, no. 2, pp. 822–835, Sep. 2015, doi: 10.1007/s10853-015-9405-2.

[8] J. M. Montes, F. G. Cuevas, J. Cintas, F. Ternero, and E. S. Caballero, "Electrical resistivity of powdered porous compacts," in *IntechOpen eBooks*, 2018. doi: 10.5772/intechopen.76159.

[9] M. Creyssels, E. Falcon, B. Castaing, M. Nakagawa, and S. Luding, "Experiment and theory of the electrical conductivity of a compressed granular metal," *AIP Conference Proceedings*, pp. 123–126, Jan. 2009, doi: 10.1063/1.3179844.

[10] M. Creyssels, C. Laroche, E. Falcon, and B. Castaing, "Pressure dependence of the electrical transport in granular materials," *The European Physical Journal E*, vol. 40, no. 5, p. 56, May 2017, doi: 10.1140/epje/i2017-11543-3.

[11] M. A. Cooper, W. W. Erikson, and M. S. Oliver, "Electrical conductivity of porous binary powder mixtures," *Mechanics of Materials*, vol. 162, p. 104026, Aug. 2021, doi: 10.1016/j.mechmat.2021.104026.

[12] P. Jop, Y. Forterre, and O. Pouliquen, "A constitutive law for dense granular flows," *Nature*, vol. 441, no. 7094, pp. 727–730, Jun. 2006, doi: 10.1038/nature04801.

[13] E. Falcon, B. Castaing, and C. Laroche, "'Turbulent' electrical transport in copper powders," *Europhysics Letters (EPL)*, vol. 65, no. 2, pp. 186–192, Jan. 2004, doi: 10.1209/epl/i2003-10071-9.

[14] E. Falcon and B. Castaing, "Electrical conductivity in granular media and Branly's coherer: A simple experiment," *American Journal of Physics*, vol. 73, no. 4, pp. 302–307, Mar. 2005, doi: 10.1119/1.1848114.

[15] Z. M. Jakšić, M. Cvetković, J. R. Šćepanović, I. Lončarević, L. Budinski-Petković, and S. B. Vrhovac, "The electrical conductance growth of a metallic granular packing," *The European Physical Journal B*, vol. 90, no. 6, Jun. 2017, doi: 10.1140/epjb/e2017-70597-6.

[16] Y. Forterre and O. Pouliquen, "Flows of dense granular media," *Annual Review of Fluid Mechanics*, vol. 40, no. 1, pp. 1–24, Jan. 2008, doi: 10.1146/annurev.fluid.40.111406.102142.

[17] P. J. Tuckman *et al.*, "Contact network changes in ordered and disordered disk packings," *Soft Matter*, vol. 16, no. 41, pp. 9443–9455, Jan. 2020, doi: 10.1039/d0sm01137a.

[18] M. Kaneta, H. Nishikawa, K. Kameishi, T. Sakai, and N. Ohno, "Effects of elastic moduli of contact surfaces in elastohydrodynamic lubrication," *Journal of Tribology*, vol. 114, no. 1, pp. 75–80, Jan. 1992, doi: 10.1115/1.2920871.

[19] M. Scaraggi and B. N. J. Persson, "Time-Dependent Fluid Squeeze-Out Between Soft Elastic Solids with Randomly Rough Surfaces," *Tribology Letters*, vol. 47, no. 3, pp. 409–416, Jun. 2012, doi: 10.1007/s11249-012-9996-6.

[20] G. Carbone, M. Scaraggi, and L. Soria, "The lubrication regime at Pin-Pulley interface in chain CVTs," *Journal of Mechanical Design*, vol. 131, no. 1, Dec. 2008, doi: 10.1115/1.3013320.

[21] M. Scaraggi and G. Carbone, "Transition from elastohydrodynamic to mixed lubrication in highly loaded squeeze contacts," *Journal of the Mechanics and Physics of Solids*, vol. 58, no. 9, pp. 1361–1373, Jun. 2010, doi: 10.1016/j.jmps.2010.05.009.

[22] G. Sivayogan, R. Rahmani, and H. Rahnejat, "Transient Analysis of Isothermal Elastohydrodynamic Point Contacts under Complex Kinematics of Combined Rolling, Spinning and Normal Approach," *Lubricants*, vol. 8, no. 8, p. 81, Aug. 2020, doi: 10.3390/lubricants8080081.

[23] R. P. Glovnea, "Transient phenomena in elastohydrodynamic lubrication," in *Recent Developments in Wear Prevention, Friction and Lubrication*, G. K. Nikas, Ed. Kerala, India: Research Signpost, 2010, pp. 227–262.

[24] B. Rallabandi, "Fluid-Elastic interactions near contact at Low Reynolds number," *Annual Review of Fluid Mechanics*, vol. 56, no. 1, pp. 491–519, Oct. 2024, doi: 10.1146/annurev-fluid-120720-024426.

[25] K. Bourbatache, M. Guessasma, E. Bellenger, V. Bourny, and A. Tekaya, "Discrete modelling of electrical transfer in multi-contact systems," *Granular Matter*, vol. 14, no. 1, pp. 1–10, Jan. 2012, doi: 10.1007/s10035-011-0307-y.

[26] C. Zeng, M. Renouf, Y. Berthier, and R. Hamdi, "Numerical investigation on the electrical transmission ability of a shearing powder layer," *Granular Matter*, vol. 18, no. 2, Mar. 2016, doi: 10.1007/s10035-016-0619-z.

[27] J. Ott, B. Völker, Y. Gan, R. M. McMeeking, and M. Kamlah, "A micromechanical model for effective conductivity in granular electrode structures," *Acta Mechanica Sinica*, vol. 29, no. 5, pp. 682–698, Oct. 2013, doi: 10.1007/s10409-013-0070-x.

[28] C. Zhang, S. Maramizonouz, D. Milledge, and S. Nadimi, "An electro-mechanical contact model for particulate systems," *Powder Technology*, vol. 440, p. 119759, Apr. 2024, doi: 10.1016/j.powtec.2024.119759.

[29] H. Hertz, "Ueber die Berührung fester elastischer Körper.," *Journal Für Die Reine Und Angewandte Mathematik (Crelles Journal)*, vol. 1882, no. 92, pp. 156–171, Jan. 1882, doi: 10.1515/crll.1882.92.156.

[30] K. L. Johnson, *Contact Mechanics*, Cambridge: Cambridge University Press, 1985. doi: 10.1017/cbo9781139171731.

[31] B. N. J. Persson, "Contact mechanics for randomly rough surfaces," *Surface Science Reports*, vol. 61, no. 4, pp. 201–227, Jun. 2006, doi: 10.1016/j.surfrep.2006.04.001.